POLITECNICO
MILANO 1863

SCUOLA DI INGEGNERIA INDUSTRIALE
E DELL'INFORMAZIONE

Executive Summary of the Thesis

Augmented Reality and Robot-Assisted Needle Insertion for Percutaneous Nephrolithotomy Task

Laurea Magistrale in Biomedical Engineering - Ingegneria Biomedica

Author: Matteo Pecorella

Advisor: Prof. Elena De Momi

Co-advisors: Junling Fu

Academic year: 2022-2023

1. Introduction

This work focuses on Percutaneous Nephrolithotomy (PCNL), considered the gold standard for treating patients with kidney stones larger than 20mm [1]. This procedure has the benefits of minimally invasive surgery, such as smaller incisions, less pain and blood loss, and shorter hospital stays [2]. It involves inserting a nephroscope into the kidney to break up a stone with ultrasounds or a laser beam and then suctioning out the pieces through one of the scope's channels. The best surgery outcome in terms of patient safety, time consumption, and stone removal, is achieved if the needle insertion position and orientation are as accurate as possible since a bad insertion could lead to harm to some organs such as the large intestine or the vessels. Thus, renal access is a crucial aspect in PCNL [1].
Despite the importance of the procedure, there are still some limitations such as the surgeon's workload and challenges in precise needle insertion. The surgeon needs to handle several jobs simultaneously such as coordination with the radiologist and nurses, and viewing the CT images taken before the operation to identify the ureter position. Accurately placing a needle based on radiological images is a challenging task due to the complexity of the procedure and difficulties with hand-eye coordination [2]. Furthermore, the procedure requires a high number of CT scans to locate the ureter and needle positions, which exposes operating room personnel to hazardous radiation.
To improve PCNL needle insertion, studies explored robotic assistance or Augmented Reality visualization. The study [2] proposed a robotic system to assist with surgical insertions, allowing the surgeon to focus on other tasks. However, the insertion planning still relied on fluoroscopic images and the fully automatic insertion makes emergency management more challenging. The study [1] adopted an AR-based solution for path planning and robotic-assisted insertion. However, the system still required fluoroscopic imaging as it doesn't include an AR-based navigation system. In the end, [3] implemented an AR-based solution for path planning and real-time navigation without fluoroscopic imaging. However, the needle insertion was done freehand.
- Motivation of the work This work aims at implementing an AR visualization-based path planning and navigation system for percutaneous nephrolithotomy with robotic guided nee-

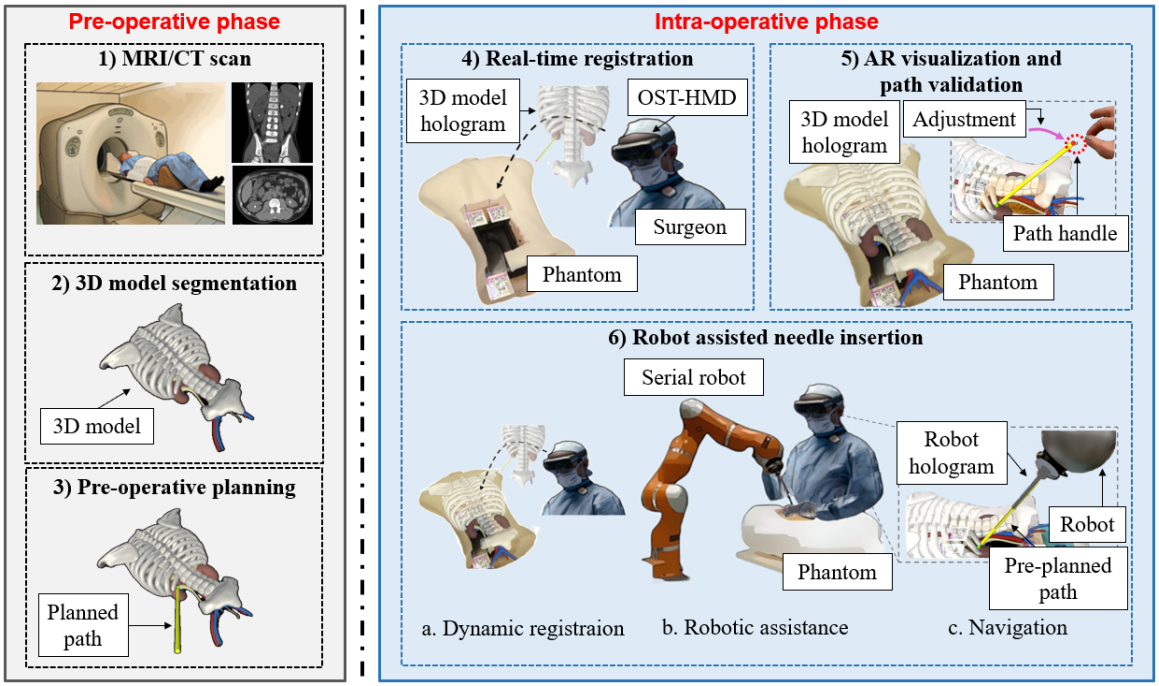

Figure 1: Overall framework of the proposed system

dle insertion. The aim is to improve the PCNL procedure workload for the surgeon and reach a good insertion accuracy.

2. Materials and methods

2.1. Proposed system architecture

The system architecture proposed in Fig. 1 is divided into two phases: the pre-operative and intra-operative phases. During the pre-operative phase, the MRI or CT scan images of the patient are segmented to generate a 3D model, and the desired path is planned accordingly. In the intra-operative phase, the surgeon uses an Optical See Through - Head Mounted Display (OST-HMD) to perform real-time registration and visualize the 3D model hologram superimposed on the patient. The surgeon then validates and adjusts the pre-planned path based on intra-operative images and is assisted by a serial robot to perform the insertion. Additionally, during the robot assisted needle insertion (Fig. 1.6) the surgeon can perform the dynamic registration to refresh the 3D model hologram position whenever it is wrong and can navigate by means of a robot hologram visualization superimposed on the real one. A demo video of the system can be found at `https://www.dropbox.com/s/4f11b7d152iqdww/AR%2BRoboticAssisted_PCNL_procedure.mp4?dl=0`.

- Coordinates Transformation and system calibration Fig. 2 shows the coordinates transformations between the components of the proposed architecture. To visualize the robot hologram and the 3D model hologram, it is essential to know the transformations from the OST-HMD to the Robot and from the OST-HMD to the Phantom, denoted as T_{Ho}^{R} and T_{Ho}^{Ph} respectively. The rest of the coordinate systems are: T_{R}^{N}, T_{N}^{Ph}, T_{N}^{T} and T_{N}^{S}, respectively represents the transformation from the robot base R to the optical tracking system (NDI Polaris Vicra, Northern Digital Inc., Canada) N, from N to human phantom Ph, from N to reference tool T, from N to surgical stylus S. As it can be seen in Fig. 2, an optical tracker has been used to compute T_{Ho}^{R}. Moreover, T_{R}^{N} is calculated with classical Eye-to-Hand calibration, while T_{Ho}^{Ph} and T_{N}^{Ph} are obtained using Singular Value Decomposition (SVD).

- OST-HMD to phantom registration The phantom registration computes T_{Ho}^{Ph} to visualise the 3D model hologram superimposed on the phantom into the correct position. This approach utilizes three QR code markers that are accurately positioned on a phantom model in relation to the ureter, see Fig. 3.

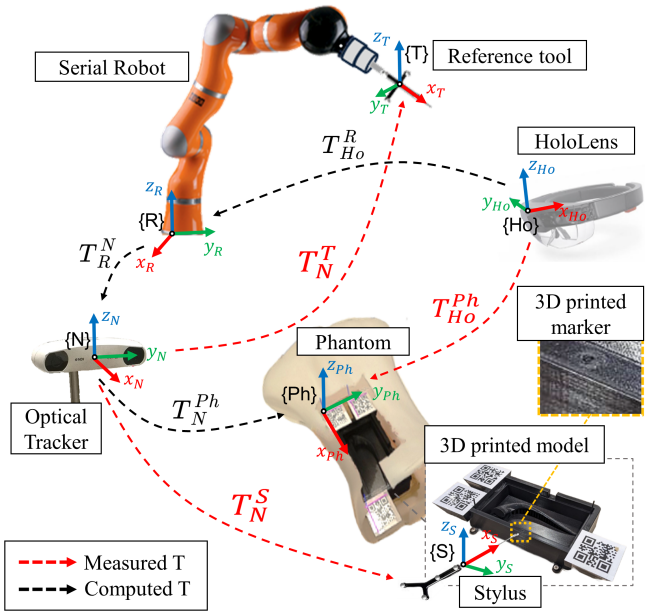

Figure 2: Coordinate transformation schema

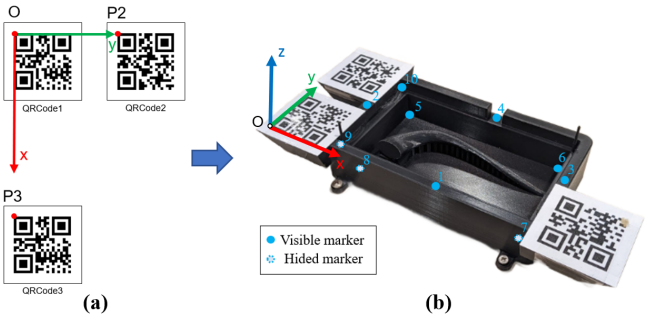

Figure 3: (a) QR markers illustration, (b) Final phantom RF and fiducial markers positions

The precise placement of these markers is achieved through the use of a ureter 3D printed model, shown in Fig. 2, placed at an exact position inside the phantom Reference Frame (RF) built over the QR codes by defining the x axis along the $O-P2$ direction, y axis along the $O-P1$ direction and the z axis as the x and y cross product. The QR code scanning feature of the HoloLens is then used to acquire the QR codes positions (O, $P2$, $P3$) and perform the paired point registration with the SVD algorithm procedure:

$$T_{Ho}^{Ph} = \text{SVD}((O_{Ho}, X_{Ho}, Z_{Ho}), (O, P2, P3)) \quad (1)$$

Where (O_{Ho}, X_{Ho}, Z_{Ho}) are the markers known position in the 3D holographic model. The result of the application of this registration is the visualization of the 3D model hologram superimposition onto the phantom.

- OST-HMD to real robot registration The robot registration computes T_{Ho}^{R} to visualize the robot hologram superimposed onto the real one (see Fig. 1.6.c) in order to implement the navigation system. This is achieved by using the Optical Tracker (OT) to measure T_R^N and T_N^{Ph}, which are then used in $T_R^{Ph} = T_R^N * T_N^{Ph}$ to calculate the coordinate transformation from the phantom to the robot. With this transformation, $T_{Ho}^{R} = T_{Ho}^{Ph} * T_{Ph}^{R}$ can be computed. Therefore, in order to compute T_{Ho}^{R}, it is necessary to measure both T_R^N and T_N^{Ph}.

- T_N^{Ph} *estimation*: is performed with the SVD paired point registration over 10 fiducial markers placed on the 3D printed phantom (see Fig. 3.b). The 10 fiducial markers' position inside the phantom RF is known M_{Ph}=$\{M1_{Ph}$, ..., $M10_{Ph}\}$, while the positions of the same fiducial markers in the OT RF {N} are measured M_N=$\{M1_N$, ..., $M10_N\}$ using the Stylus (Fig. 2). Each Mi_N $(i = 1, ..., 10)$ position is acquired by averaging 50 OT acquisitions of the Stylus tooltip position when its placed on the i-th marker, to have a more reliable measure by averaging out the noise.
T_N^{Ph} is then computed as T_N^{Ph}=SVD(M_N, M_{Ph}).

- T_R^N *estimation*: implements the Hand-Eye calibration with the following mathematical computations. The T_R^N can be computed as

$$T_R^N = T_R^{EE} * T_{EE}^{T} * T_T^N \quad (2)$$

Where T_{EE}^{T} represents the transformation from the robot end effector (EE) to the reference tool which is mounted on the robot (see Fig. 4). T_T^N is the transform from the reference tool to the OT as detected from the OT itself. T_R^{EE} is the transform from the robot base to the EE and is given by the robot configuration. By moving the robot to different configurations, the following equation can be obtained:

$$_2T_T^R * {}_1T_T^{R-1} * T_N^R = T_N^R * {}_2T_N^{T-1} * {}_1T_N^T \quad (3)$$

the equation 3 is in the form $AX = BX$ where $A = {}_2T_T^R * {}_1T_T^{R-1}$, $B = {}_2T_N^{T-1} * {}_1T_N^T$ and the variable to be find is $X = T_N^R$. After moving the robot to several configurations, a set of equations in the format of equation 3 is obtained.

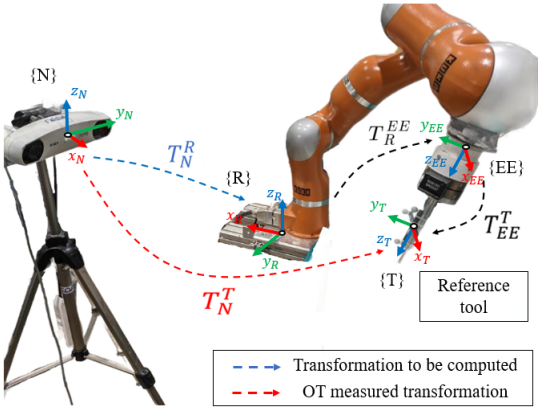

Figure 4: Eye-to-Hand calibration RF's

Tsai's algorithm is adopted to solve the above equation.

- Robotic assistance implementation In this section, the robot control strategy is developed for the robotic assistance. The details are summarized in the following steps (See Fig. 5):

Stage-1: Free Manipulation for Alignment: Firstly, the operator can manipulate freely and align the needle to the pre-planned path, visualized in AR.

Stage-2: Alignment and Stiffing of Robot: Once the operator confirms the alignment between the path and the robot hologram needle (see Fig. 5), by selecting the "Aligned" button on the OST-HMD's GUI, the robot stiffness changes.

Stage-3: Robotic assistance for Puncture: After changing stiffness, the robot assists the surgeon in performing the needle puncture procedure only along the pre-planned direction, utilizing the Cartesian impedance controller:

$$K\delta x(t) + D\dot{x}(t) = F_{ext} \tag{4}$$

The equation 4 describes the motion of the robot's EE in response to the external force F_{ext}, $\delta x(t) = (x(t) - x_0)$ is the displacement of the EE from the initial position x_0 at time t and $\dot{x}(t)$ is the velocity of the EE. **D** and **K** are constants damping and stiffness parameters of the robot.

2.2. Experimental validation

Fig. 6 shows the utilization of the HoloLens 2 (Microsoft, WA, USA) for Augmented Reality visualization, while the 7-DoFs robotic manipulator (LWR 4+, KUKA, Germany) is employed for providing assistance during percutaneous nephrolithotomy procedures. Additionally, the optical tracking system (NDI Polaris Vicra, Northern Digital Inc., Canada), as previously mentioned, is utilized for system calibration and to measure the accuracy, see Fig. 4.

To evaluate the performance of the system and the distinct impact of the AR visualization and robotic assistance 4 different system setups have been implemented and compared: (1) screen-based manual setup (SM), (2) AR-based manual setup (AM), (3) screen-based + robot assistance setup (SA), and (4) AR-based + robot assistance setup (AA). The tests were performed by a total of 14 users (6 females and 8 males, aged between 22-27 with Avg = 24.2, Std = 1.21) with no surgery or AR headsets experience. To validate the system's usability and performance each user was asked to perform the same needle insertion procedure with all 4 setups, in random order, each setup repeated 3 times.

To implement the robotic assistance, specific values are used for the parameters in equation 4. The parameter D is set to 0.707, which is the critical damping value. The parameter K is defined with respect to the EE axis (see Fig. 3) and takes on the values of 4500 N/m for the x and y axes, and 1 N/m for the z axis linear displacement and the value of 200 Nm/rad for all the axis rotational displacements. Moreover, x_0 is updated to the new EE position every time it is moved. This update occurs only along the EE's z axis.

In the end, the users' insertion accuracy was measured alongside a questionnaire filling, to obtain a qualitative evaluation of the user's workload during the tasks. Fig. 6 shows the "AA" setup steps followed during the user tests.

2.3. Performance metrics

The performance metrics evaluate the main parts of the system: (i) the phantom registration, (ii) the robot registration, (iii) the insertion procedure accuracy, and (iv) the usability.

i. Phantom registration This step's accuracy has been assessed by measuring the positioning error between 4 physical printed markers (see Fig. 7) and their holographic couple [4]. This measurement has been done 3 times and the errors were averaged. This procedure has been carried on with the OT already used in the system and consisted in the following steps:

1. Printed markers positions ($M_{Ph} = (M1_{Ph}$, $M2_{Ph}$, $M3_{Ph}$, $M4_{Ph})$) acquisition with the

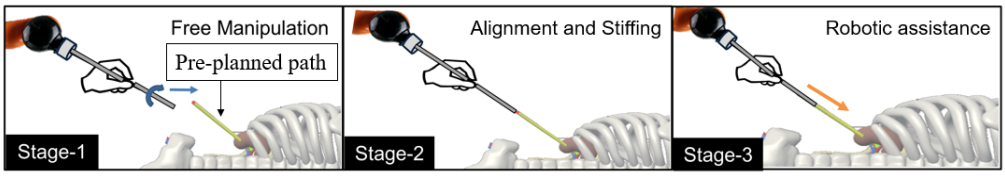

Figure 5: Robotic assistance strategy schema

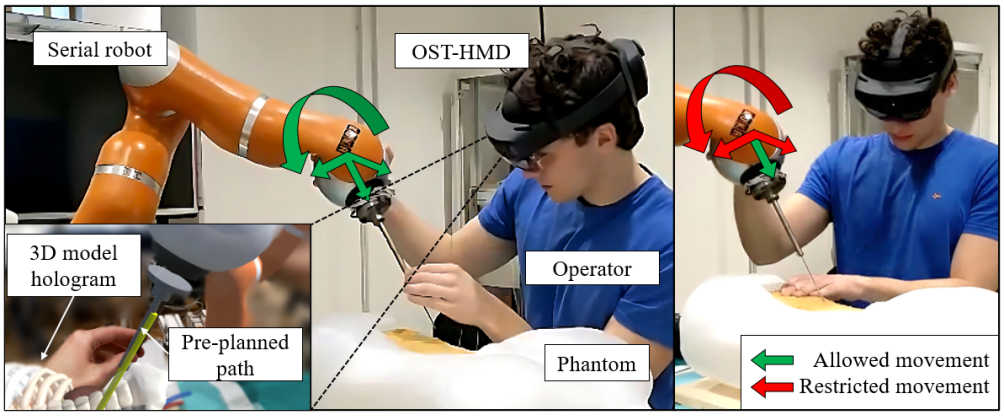

(a) Free manipulation and alignment (b) Assisted insertion

Figure 6: Details and system components of the proposed framework

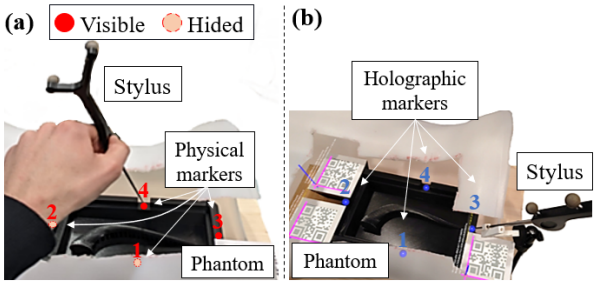

Figure 7: (a) Physical markers positions acquisition; (b) Holographic markers positions acquisition

stylus (see Fig. 7.a).

2. QR code scanning and performance of the phantom registration and visualization of the holographic markers
3. Holographic markers positions (M_{Ho} = ($M1_{Ho}$, $M2_{Ho}$, $M3_{Ho}$, $M4_{Ho}$)) acquisition with the stylus (see Fig. 7.b).

Once M_{Ph} and M_{Ho} have been acquired the single markers Euclidian error have been computed as $E_i = \|Mi_{Ph} - Mi_{Ho}\|$, i = 1,...,4.
Afterwards, the registration error for each point of the ureter has been computed. The transformations T_{OT}^{Ph} and T_{OT}^{Ho} have been estimated using SVD over M_{Ph} and M_{Ho}, respectively. Then, a set of N ureter vertices (v_j, j=1,..., N) with known position inside the phantom have been mapped by using T_{OT}^{Ph} and T_{OT}^{Ho}. Each vertex placement error has been computed as $d_j = \|T_{OT}^{Ph} * v_j - T_{OT}^{Ho} * v_j\|$. Then the RMSE over all the vertices has been computed: $RMSE = \sqrt{\frac{1}{N}\sum_{j=1}^{N} d_j}$.

ii. Robot registration To evaluate T_{Ph}^{R}, the known position of the printed markers in the phantom (Mi_{Ph}) is measured from the robot by positioning the tooltip on the marker (Mi_R) [5]. The i-th marker positioning error can be computed as $E_i = |Mi_R - T_{Ph}^{R} \cdot Mi_{Ph}|$ and the final RMSE is computed over 4 markers as $RMSE = \sqrt{\frac{E_1^2+E_2^2+E_3^2+E_4^2}{4}}$.

iii. Insertion procedure The insertion accuracy has been evaluated over the orientation error (E_O) with respect to the reference path and the translation error (E_T) between the target and the tooltip final position projection (Fig. 8) [1], [5]. E_O and E_T are computed by:

$$\begin{aligned} E_O &= acos\left(\frac{\vec{v}_{planned} \cdot \vec{v}_{real}}{\|\vec{v}_{planned}\| \cdot \|\vec{v}_{real}\|}\right) \\ P &= |\vec{v}_{planned}| \cdot cos(E_O) \cdot \vec{v}_{real} \\ E_T &= \|P - T\| \end{aligned} \tag{5}$$

Where, $\vec{v}_{planned}$ represents the reference path, $\vec{v}_{real}$ the real insertion path, E_O the angle be-

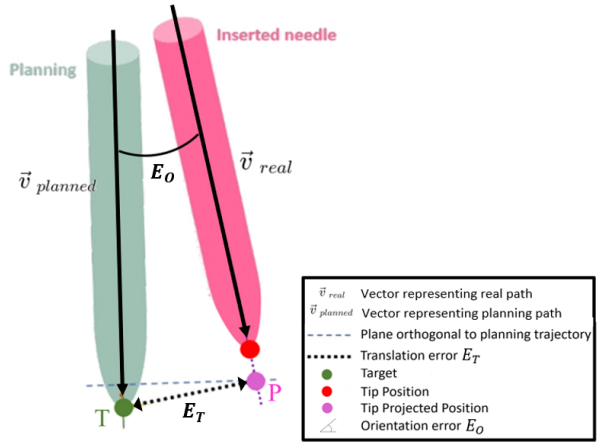

Figure 8: Insertion error computation schema

Performance	SM	SA	AM	AA
E_T [mm]	6.6 ± 1.1	6.2 ± 3.1	7.4 ± 3.6	$\mathbf{3.2 \pm 1.4}$
E_O [°]	2.8 ± 0.6	1.8 ± 1.4	3.2 ± 1.8	$\mathbf{1.2 \pm 0.9}$
Time [s]	218 ± 50	165 ± 82	100 ± 55	$\mathbf{171 \pm 109}$

Table 1: Translation and Orientation errors and execution time

tween the two vectors, and E_T is the Euclidian distance between P and T. Alongside E_O and E_T, the execution time has been measured.

iv. System usability The effort required to use a system defines its usability. To prove that using robotic assistance improves system usability compared to only using AR, a statistical analysis over the NASA Task Load Index (NASA-TLX) was conducted.

3. Results

- Phantom registration The above procedure repeated 3 times gave the median Euclidian distances of the 4 markers $E_1 = 3.19$ mm, $E_2 = 1.78$ mm, $E_3 = 3.63$ mm and $E_4 = 3.60$ mm. Then the point-to-point accuracy over the whole model as obtained from the RMSE formula showed a result of 2.44 mm. An acceptable value if compared to other studies such as [4] that present 3.19mm.

- Robot registration The RMSE computed as stated above gave a value of 1.49mm. This value results to be better than some studies that don't implement the OT, such as [5] that presents an average value of 3.36 mm.

- Insertion procedure E_O, E_T and execution time mean and standard deviation for each system setup are summed up in Table 1. The experimental results are shown in Fig. 9 with the

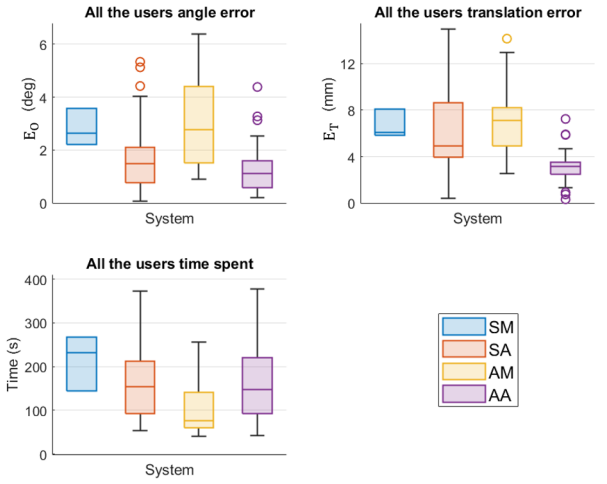

Figure 9: Performance metrics comparison results for needle insertion task

Error	Setup	SM	SA	AM
E_O	AA	$1.8 \cdot 10^{-11}$	0.047	$1.5 \cdot 10^{-8}$
E_O	SA	$9.6 \cdot 10^{-7}$	–	$3.1 \cdot 10^{-4}$
E_T	AA	$2.5 \cdot 10^{-13}$	$1.3 \cdot 10^{-7}$	$1.6 \cdot 10^{-10}$
E_T	SA	0.016	> 0.05	> 0.05
Time	AA	0.0011	> 0.05	$4.3 \cdot 10^{-4}$
Time	SA	0.0011	$1.3 \cdot 10^{-4}$	$4.3 \cdot 10^{-4}$
Time	SM	–	0.0011	$2.7 \cdot 10^{-10}$

Table 2: Experimental results p-values

related p-values shown in Table 2, where only the meaningful p-values are indicated, the omitted p-values were higher than 0.05, which is the statistical significance threshold.

- System usability Fig. 10 reports the NASA-TLX scores for all 4 setups. The indicated score is the result of the sum of the NASA-TLX categories (Mental Demand, Physical Demand, Temporal Demand, Performance, Effort and Frustration) scores, scaled in the interval [0,100] where a low score means less workload during tasks. Table 3 shows the p-values of the NASA-TLX combined scores boxplot p-values, showing the statistically relevant comparisons. Table 4 reports the median and standard deviation values of the NASA-TLX overall score.

Setup	SM	SA
AA	0.0032	0.0073
AM	0.0045	0.0190

Table 3: Comparison results of different modalities with NASA-TLX overall score p-values

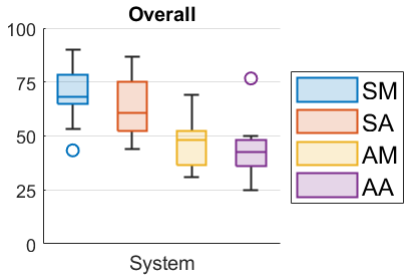

Figure 10: User questionnaire scores

Category	SM	SA	AM	AA
Overall	67.9 ± 13.8	60.8 ± 14	47.9 ± 10.8	$\mathbf{42.5 \pm 10.73}$

Table 4: NASA-TLX user evaluation experimental results

4. Discussion

The insertion procedure accuracy results show that the setup implementing both AR and robotic assistance has smaller orientation and translation errors, reaching an accuracy of 3.2 $\pm$ 1.4 mm in translation and 1.2 $\pm$ 0.9° in orientation. This accuracy is better than [1] and [5], and comparable to [3], which shows that both AR and robotic assistance improved the performance for this task.
The system usability results show that the method with both AR and robotic assistance is the most usable one, followed by the "AM" setup that demonstrates that AR brings bigger benefits to the system usability compared to robotic assistance. All the system setups show better results compared to the standard operating room PCNL procedure "SM" both from the accuracy and usability point of view.
The analysis concludes that both the AR and robotic assistance return a positive contribution in terms of the usability of the system and not only from the performance point of view. However, some possible limitations of the work could be found, in particular the increased system complexity introduced with respect to the standard PCNL procedure setup, the limited preliminary user testing conducted on the system, and the user discomfort caused by the HoloLens.

5. Conclusion

This paper presents a novel framework, which combines AR with a robotic system to improve the surgeon's performance during a percutaneous nephrolithotomy (PCNL) needle insertion procedure. The system is particularly useful for surgeries that require a very accurate needle insertion with respect to a pre-planned path such as PCNL. Therefore, the proposed system can be adapted for other surgical procedures.
Possible future works aim to improve hologram stability, user comfort, and patient respiratory motion compensation. An extensive evaluation with different groups of users and expert surgeons is planned to be implemented. The performances of surgeons with and without the assistance of our proposed system will be compared to validate its overall effectiveness.

References

[1] Federica Ferraguti, Marco Minelli, Saverio Farsoni, Stefano Bazzani, Marcello Bonfè, Alexandre Vandanjon, Stefano Puliatti, Giampaolo Bianchi, and Cristian Secchi. Augmented reality and robotic-assistance for percutaneous nephrolithotomy. *IEEE robotics and automation letters*, 5(3):4556–4563, 2020.

[2] Hsieh-Yu Li, Ishara Paranawithana, Zhong Hoo Chau, Liangjing Yang, Terence Sey Kiat Lim, Shaohui Foong, Foo Cheong Ng, and U-Xuan Tan. Towards to a robotic assisted system for percutaneous nephrolithotomy. In *2018 IEEE/RSJ International Conference on Intelligent Robots and Systems (IROS)*, pages 791–797. IEEE, 2018.

[3] Lei Wang, Zichen Zhao, Gang Wang, Jianfang Zhou, He Zhu, Hongfeng Guo, Huagang Huang, Mingchuan Yu, Gang Zhu, Ningchen Li, et al. Application of a three-dimensional visualization model in intraoperative guidance of percutaneous nephrolithotomy. *International Journal of Urology*, 29(8):838–844, 2022.

[4] Maria Chiara Palumbo, Simone Saitta, Marco Schiariti, Maria Chiara Sbarra, Eleonora Turconi, Gabriella Raccuia, Junling Fu, et al. Mixed reality and deep learning for external ventricular drainage placement: A fast and automatic workflow for emergency treatments. In *MICCAI 2022: 25th International Conference, Singapore, September 2022, Part VII*.

[5] Viktor Vörös, Ruixuan Li, Ayoob Davoodi, Gauthier Wybaillie, Emmanuel Vander Poorten, and Kenan Niu. An augmented reality-based interaction scheme for robotic pedicle screw placement. *Journal of Imaging*, 8(10):273, 2022.